ACS APPLIED MATERIALS & INTERFACES

Research Article

www.acsami.org

Diffusion-Controlled Growth of Molecular Heterostructures: Fabrication of Two-, One-, and Zero-Dimensional C_{60} Nanostructures on Pentacene Substrates

Tobias Breuer and Gregor Witte*

Molekulare Festkörperphysik, Philipps-Universität Marburg, D-35032 Marburg, Germany

Supporting Information

ABSTRACT: A variety of low dimensional C_{60} structures has been grown on supporting pentacene multilayers. By choice of substrate temperature during growth the effective diffusion length of evaporated fullerenes and their nucleation at terraces or step edges can be precisely controlled. AFM and SEM measurements show that this enables the fabrication of either 2D adlayers or solely 1D chains decorating substrate steps, while at elevated growth temperature continuous wetting of step edges is prohibited and instead the formation of separated C_{60} clusters pinned at the pentacene step edges occurs. Remarkably, all structures remain thermally stable at room temperature once they are formed. In addition the various fullerene structures have been overgrown by an additional pentacene capping layer. Utilizing the different probe depth of XRD and NEXAFS, we found that no contiguous pentacene film is formed on the 2D C_{60} structure, whereas an encapsulation of the 1D and 0D structures with uniformly upright oriented pentacene is achieved, hence allowing the fabrication of low dimensional buried organic heterostructures.

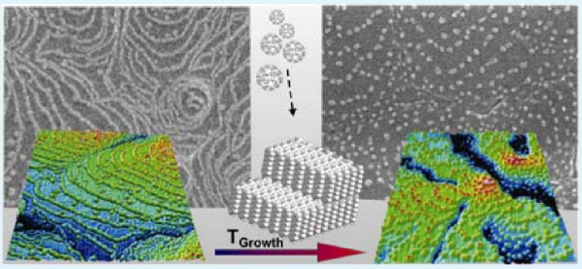

KEYWORDS: *organic semiconductors, organic heterostructures, diffusion, nanostructuring, pentacene, C_{60}, atomic force microscopy, near-edge X-ray fine structure spectroscopy*

INTRODUCTION

Low dimensional semiconductor heterostructures have been the subject of intense research because they enable electron confinement and exhibit new transport properties that are useful for device applications.[1,2] In contrast to such inorganic semiconductor structures, which can be specifically fabricated by means of molecular beam epitaxy in combination with lithography based structuring methods, heterostructures consisting of organic semiconductors are studied far less thoroughly. Present efforts to prepare molecular nanostructures are mostly limited to hybrid systems such as self-assembled monolayers,[3,4] nanoparticles coated by ligand shells,[5,6] or block copolymer micelles.[7] A commonly used strategy to fabricate 2D molecular nanostructures is based on the surface science approach where a large variety of structures has been observed for monolayer films chemisorbed at metal substrates[8,9] that result from supramolecular association and substrate template effects. Though template controlled growth can be used to prepare long-range ordered monolayers with uniaxial molecular orientation,[10−12] such structural motifs are usually not transferred to multilayer films.[13] This limitation can be rationalized by rather different molecular interactions acting within the film and toward the substrate: while molecules are fixated by chemical bonds at the surface, they experience only weak, essentially van der Waals type mutual interactions. As a consequence, multilayer structures generally exhibit a larger degree of imperfection and strongly reduced thermal stability compared to chemisorbed monolayers. In the case of molecular heterostructures the situation is even more complex because unequal interactions between the different molecular entities may cause phase separation upon growth.[14,15] On the other hand the weak intermolecular interaction in purely van der Waals bond solids favors notable interdiffusion already at room temperature and can lead to substantial intermixture of sequentially deposited molecular films[16] that might hamper the formation of well separated molecular heterolayers. To date, only few examples of ordered molecular heterostructures have been reported, essentially showing orientational control in vertically stacked layers.[17−21] By contrast dimensionality effects in molecular semiconductors are yet widely unexplored though this topic might provide challenging perspectives for future applications.[22]

The promising potential of organic photovoltaic (OPV) devices based on acceptor−donor heterojunctions of conjugated polymers and/or oligomers has recently attracted substantial research interest in such interfaces. To improve the understanding of the microstructure and energetics of molecular heterostructures, prototypical model interfaces between small molecular weight organic compounds that form crystalline films, such as fullerene (C_{60}) and pentacene,

Received: July 17, 2013
Accepted: September 4, 2013
Published: September 4, 2013

are of particular interest.[23,24] Especially for pentacene/C60 based photovoltaic cells the occurrence of singlet exciton fission has recently been demonstrated to enhance the potential quantum efficiency significantly by breaking the Shockley–Queisser limit.[25] Moreover, this particular binary material combination has been successfully used to fabricate ambipolar organic field effect transistors.[26] Previous studies have shown that pentacene/C_{60} blends prepared by coevaporation reveal phase separation.[27,28] In contrast, the formation of well ordered network or pinwheel structures was found upon cocrystallization of monolayers on metal substrates,[29,30] while deposition of C_{60} onto pentacene films yields clusters pinned at pentacene step edges.[31] The complexity of such structural motifs has also triggered significant theoretical efforts to analyze pentacene/C_{60} interfaces.[32−35] In addition, detailed energy calculations indicate that the electronic coupling between pentacene and C_{60} depends significantly on their relative molecular orientation which has important implications for electronic devices employing such heterojunctions.[36,37] However, the complexity of pentacene/C60 heterostructures has so far hampered detailed experimental studies on well-defined interfaces which are mandatory for surveying intermolecular coupling.

In this study, we have extensively analyzed the growth of C_{60} layers onto (001)-oriented pentacene films by combining atomic force microscopy (AFM), scanning electron microscopy (SEM), X-ray diffraction (XRD), and X-ray absorption spectroscopy (NEXAFS). A systematic variation of the growth conditions shows that at appropriate substrate temperatures rather different C_{60} structures can be fabricated: at cryogenic temperatures homogeneous wetting occurs yielding 2D C_{60} films, while with increasing growth temperature the fullerenes diffuse toward step edges of the pentacene layer and form 1D chains. By contrast, growth of C_{60} at or above room temperature causes dewetting and formation of separate C_{60} clusters that nucleate at pentacene step edges.[38] In addition we have also addressed the topic of whether the various C_{60} structures can be overgrown by pentacene films in order to fabricate buried heterostructures. The different probe depth of XRD and NEXFAS provides detailed information about the orientational ordering of bottom and top pentacene layers and shows that fullerene chains and clusters can be well overgrown by a crystalline pentacene capping layer that maintains upright molecular orientation.

EXPERIMENTAL SECTION

The thin films of pentacene (Sigma Aldrich, purity ≥99.9%) and C_{60} (Sigma Aldrich, purity ≥99.5%) were grown under ultrahigh-vacuum (UHV) conditions by organic molecular beam deposition (OMBD) from alumina crucibles of resistively heated Knudsen cells. By use of cell temperatures of 500 and 650 K for pentacene and C_{60}, respectively, typical deposition rates of 6 Å/min (pentacene) and 2 Å/min (C_{60}) were achieved that were monitored by quartz crystal microbalance (QCM). The films were grown onto natively oxidized Si(100) substrates which were cleaned by rinsing with ethanol, followed by heating in UHV to 600 K for 30 min.

The film morphology was characterized by atomic force microscopy (AFM, Agilent SPM 5500) operated in tapping mode at ambient conditions and room temperature. AFM tips with resonance frequencies of about 260 kHz, radii of 7 nm, and force constants of 26.1 N/m were used. Scanning electron microscopy (SEM, Jeol JSM-7500F operated at 20 kV acceleration voltage) was applied to obtain additional, complementary information about the lateral ordering of the interface.

NEXAFS measurements were carried out at the HE-SGM dipole beamline at the synchrotron storage ring facility BESSY II in Berlin, Germany. The spectra were recorded by measuring the secondary partial electron yield as function of the photon energy of the linearly polarized incident synchrotron light (polarization factor 91%). Moreover, the polarization dependency of resonant excitations from C 1s core levels into unoccupied π orbitals (π^* resonances) can be used to characterize the molecular orientation because their intensity depends on the orientation of the electrical field vector $\vec{E}$ of the incident synchrotron light relative to the molecular transition dipole moment $\vec{T}$ according to $I \propto |\vec{E}\cdot\vec{T}|^2$. For π^* excitations, $\vec{T}$ is oriented normal to the ring plane of the aromatic moieties, hence enabling a determination of their orientation relative to the sample normal from angular dependent NEXAFS measurements taken at different angles of incidence (so-called dichroism). Note that this analysis does not require any crystalline ordering. Moreover, the partial electron yield mode is highly surface sensitive, hence providing structural information in the first few layers which is an important advantage over XRD. More details on the experimental setup and the data analysis are presented in the Supporting Information.

The crystalline orientation of selected samples was determined from XRD data acquired with a diffractometer (Bruker D8 Discovery) using Cu Kα radiation (λ = 1.540 56 Å) and a LynxEye detector.

RESULTS AND DISCUSSION

To provide well-defined pentacene substrates with uniform molecular orientation and to exclude competing interaction of fullerenes with the supporting substrate, which might affect the film structure,[39] all C_{60} films were deposited onto 30 nm pentacene bottom layers that had been grown on SiO_2 at room temperature. In accordance with previous studies, such pentacene layers crystallize in the thin film phase and form (001)-oriented films.[40] As shown by the AFM micrograph in Figure 1a, they consist of coalesced single crystalline grains of a width of few micrometers and exhibit atomically flat terraces extending over 100−200 nm separated by monomolecular steps, yielding an overall rms roughness of less than 5 nm (for additional XRD data, see Supporting Information, Figure S5). Since previous work revealed severe tip-induced film modifications upon imaging of molecular multilayer films by scanning tunneling microscopy, owing to their low conductivity,[41] we instead used AFM to characterize the morphology of the molecular heterostructures.

Figure 1b displays the interface formed by deposition of small C_{60} amounts (d_{nom} = 0.25 nm)[42] at room temperature onto the pentacene bottom layer, yielding small C_{60} clusters that are exclusively pinned at pentacene step edges. To accentuate the lateral distribution of these clusters and to decouple the superimposed height variation due to pentacene substrate terraces, we present amplitude images of the AFM data shown in false colors, while line scans represent the corresponding topography (details in Supporting Information). The observed step decoration reflects enhanced adsorption energy of C_{60} molecules on pentacene step edges as compared to terrace sites which is in line with recent force field based MD simulations.[33] Interestingly, another theoretical study on the growth of C60 on pentacene substrates found a notable indiffusion of fullerenes at step edges which suggests an alternative mechanism for the preferential nucleation of C60 islands at step edges.[35] As the precise determination of the cluster size might be limited by the resolution of the AFM due to the finite tip apex, additional SEM measurements have been performed at the identical samples (cf. Figure 1e), additional micrographs in Supporting Information Figure S4). The quantitative analysis combining the lateral dimensions of the clusters determined by SEM and height information provided by AFM yields cluster diameters of about 25 nm and a height of

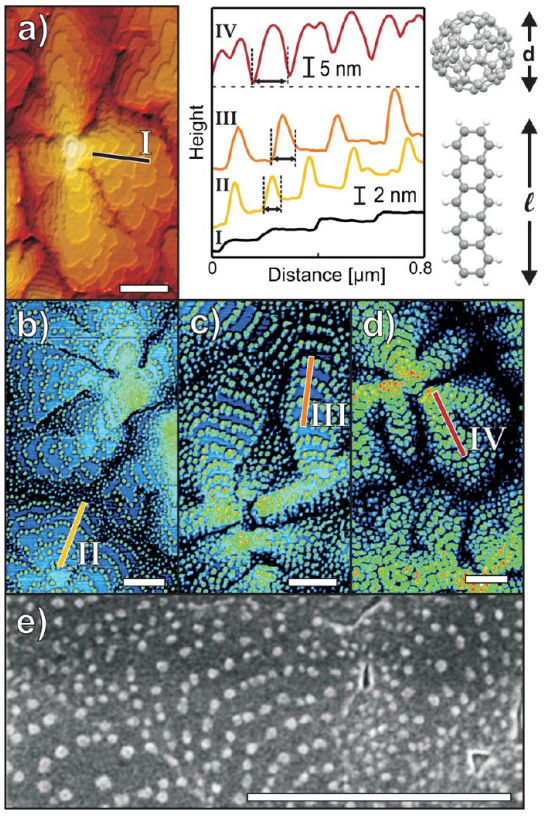

Figure 1. AFM micrographs showing (a) the morphology of the 30 nm pentacene bottom layer and the amplitude images after C_{60} deposition of various nominal thickness at room temperature, (b) 0.25 nm, (c) 0.5 nm, and (d) 5 nm together with corresponding line scans showing the height profile of the films. Panel e shows SEM micrographs of sample c. All scale bars correspond to 0.5 μm.

4−6 nm. These values are much larger than the van der Waals diameter of fullerenes (1.0 nm) and therefore indicate agglomeration of the fullerenes. Doubling the amount of deposited C_{60} (d_{nom} = 0.5 nm) still reveals no nucleation on the terraces and, surprisingly, does not result in continuous decoration of the step edges but leads to clusters of increased height (8−10 nm) and diameter (40 nm). To monitor the film evolution at a later stage, also explicitly higher amounts of C_{60} (d_{nom} = 5 nm) were deposited onto the pentacene bottom layer. Even for this coverage (which corresponds to six nominal layers of densely packed C_{60} molecules), individual C_{60} clusters can be recognized that have further extended in size (up to 15 nm in height, about 80 nm in diameter) and are partially coalesced, resulting in significant film roughness. The formation of individual C_{60} clusters coexistent with notable regions of undecorated step edges indicates that the C_{60} cohesion exceeds the C_{60}−pentacene adhesion.

Moreover, it shows that upon room temperature deposition C_{60} diffusion at terraces and along step edges is activated. Considering further the different adsorption energy of C_{60} on (001)-terraces and step edges of pentacene, it appears conceivable to control the diffusion length on terraces and steps separately by the substrate temperature. To test this hypothesis and to better understand the dynamics of step edge decoration, additional C_{60} films (in each case with a fixed nominal thickness of 0.5 nm) were grown on pentacene bottom layers at different substrate temperatures ranging from 145 to 345 K. Interestingly, a continuous evolution of the growth of C_{60} on pentacene is found as summarized in Figure 2. While rather homogeneous coating of the pentacene terraces occurs for fullerene deposition at 145 K (which is also found for higher C_{60} thicknesses, cf. Supporting Information, Figure S2), at somewhat elevated temperatures coexistence between terrace growth and step edge decoration is present. Further elevation of the subtrate temperature to 240 K yields continuous step edge decoration without observable gaps between the C_{60} clusters along the step edges. The initially mentioned more discrete step edge decoration with enhanced individual cluster heights at room temperature becomes even more pronounced at 345 K during C_{60} evaporation. In this case, large regions of the step edges remain uncovered while the higher diffusivity of the C_{60} molecules on uprightly oriented pentacene[43] at elevated substrate temperature supports the formation of clusters of more than 9 nm in height. Measurements at higher substrate temperatures have not been carried out to avoid thermally

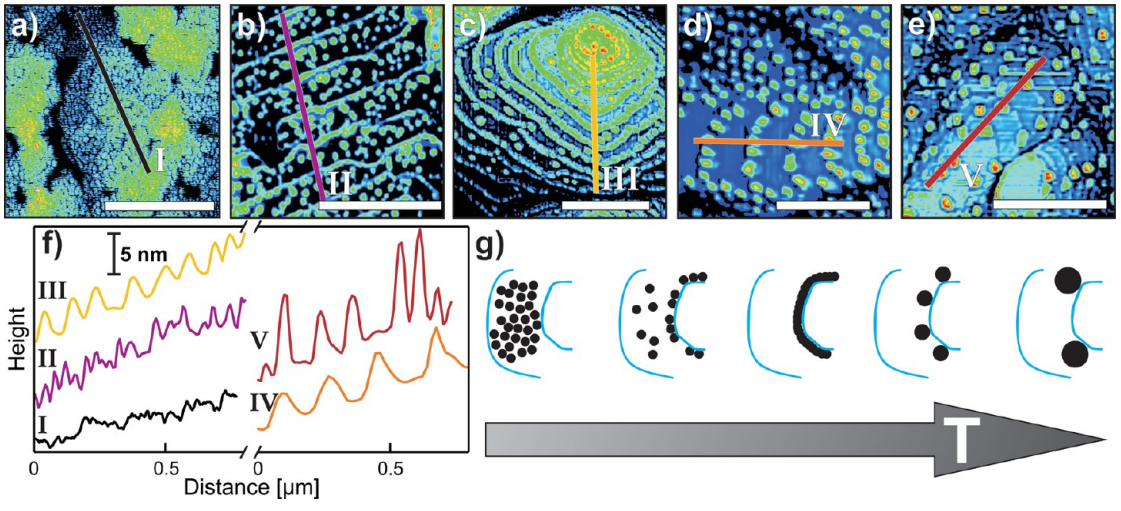

Figure 2. Summary of AFM micrographs showing the resulting heterostructures obtained by deposition of 0.5 nm C_{60} onto a 30 nm (001) oriented pentacene bottom layer at different substrate temperatures, (a) T = 145 K, (b) T = 170 K, (c) T = 240 K, (d) T = 300 K, and (e) T = 345 K, together with (f) corresponding line scans of the height profiles and (g) schematic representation of the formed C_{60} structures as function of the substrate temperature during C_{60} deposition. All scale bars correspond to 0.5 μm.

dx.doi.org/10.1021/am402868s | ACS Appl. Mater. Interfaces 2013, 5, 9740−9745

activated roughening or even desorption of the pentacene bottom layer.[44]

Interestingly, the various film morphologies are fully maintained at room temperature where all micrographs have been acquired. We note further that no evidence was found for any morphological changes after deposition by comparing samples that have been quickly transferred out of the vacuum chamber to those that have been prepared at low temperatures and postannealed to higher temperatures or stored for several days under UHV at room temperature. This behavior is quite different from the case of pentacene where a pronounced postdeposition dewetting occurs.[44] It demonstrates that C_{60} layers are thermally rather stable once a certain island size is reached which prevents subsequent diffusion. This observation is well rationalized by a recent computational study of the diffusion of C_{60} on pentacene which showed that the diffusion coefficients decrease rapidly when instead of single molecules small fullerene clusters are moving over the pentacene surface.[32] Conclusively, our results show that the diffusivity of C_{60} is sufficient to decorate the step edges of pentacene even at temperatures as low as 170 K, which is quite surprising regarding the high molecular mass and the high thermal stability of solid C_{60}. By contrast, smooth interfaces with homogeneous coverage are found at cryogenic growth temperatures, where even diffusion on the terraces is thermally not activated and fullerenes freeze out upon deposition, while the interface roughness increases with deposition temperature yielding only a small contact area at high temperatures (cf. Figure 2g). Comparing the different nucleation scenarios, one can assign different dimensionalities to the resulting C_{60} films: low substrate temperatures during C_{60} deposition cause planar covering of the pentacene surface and yield quasi-2D structures, while at 240 K essentially only the pentacene step edges are covered homogeneously (1D covering) and at elevated temperatures (345 K) separated 0D clusters are formed.

In a next step, we were also interested in the consequences of further pentacene deposition onto the various heterostructures, aiming at the preparation of buried C_{60} structures. For this purpose, a 5 nm pentacene capping layer was deposited at room temperature onto the various C_{60}/pentacene heterostructures (0.5 nm C_{60} on 30 nm pentacene), where C_{60} had been deposited at different substrate temperatures of 145, 240, and 300 K, respectively. Figure 3a–c summarizes the corresponding AFM micrographs of the resulting structures. On the 2D C_{60} layer rather small but tall pentacene islands are formed that reveal elevations of about 10–15 nm relative to the C_{60}/pentacene underlayer. Interestingly, some areas between the pentacene islands exist where the uncovered C_{60} film remains visible, hence reflecting incomplete wetting (white boxes in Figure 3a).

When pentacene is deposited on C_{60} chains, a significantly different morphology is found. The capping layer has clearly reduced roughness and consists of extended islands that exhibit characteristic molecular steps that correspond to upright molecular orientation. In contrast to the morphology of the bare pentacene bottom layer (cf. Figure 1a), the pentacene adlayer reveals additional steps and grain boundaries on the terraces of the bottom layer, in some cases even orthogonal to the substrate step edge direction (see Figure 3b). Their formation might be related to the step decoration which is expected to reduce the diffusion of pentacene admolecules, hence causing additional nucleation.

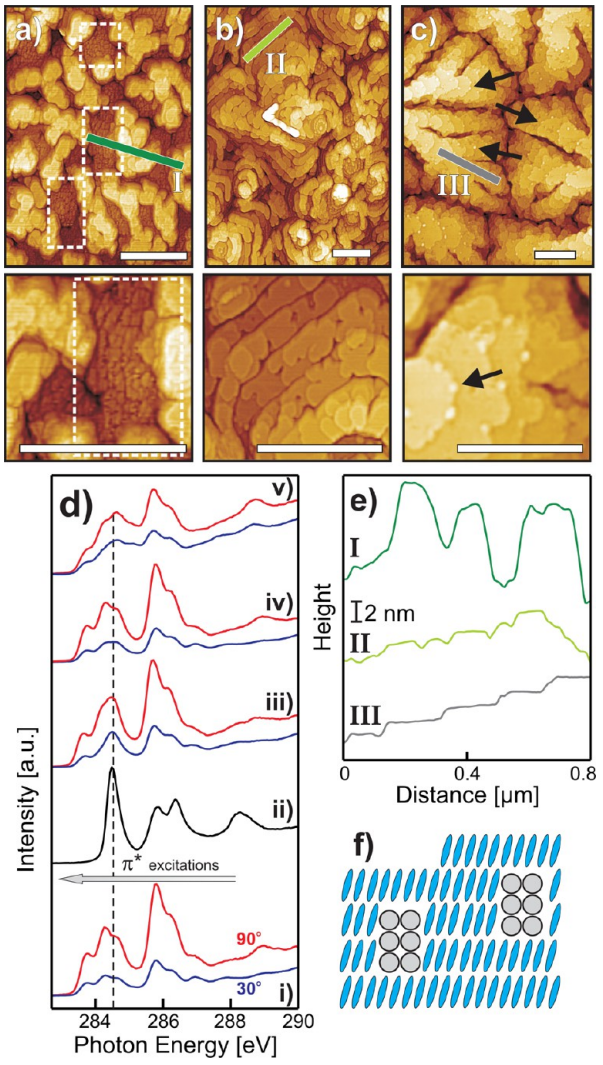

Figure 3. AFM micrographs showing the morphology of 5 nm pentacene capping layers grown on C_{60} nanostructures of different dimensionality: (a) 2D, (b) 1D, (c) 0D C_{60} nanostructures, with magnifications and corresponding line scans in panel e. Panel d shows C 1s NEXAFS spectra of (i) pure pentacene thin film, (ii) pure C_{60}, (iii) 0.5 nm C_{60} on pentacene, (iv) pentacene on 0D C_{60} interface (sample like in panel c), (v) pentacene on 2D C_{60} interface (sample like in a)) together with (f) schematic illustration of growth mode of pentacene on the 0D C_{60} interface. All scale bars in AFM micrographs correspond to 0.5 μm.

Overgrowing the C_{60} clusters by pentacene yields a surface morphology that is very similar to that of the bare pentacene film (cf. Figure 1a). Dendrites of similar morphology are found as well as typical monomolecular steps of 1.5 nm as depicted in Figure 3c. Because of the large fullerene cluster size of about 8 nm, some of them are not completely buried by the 5 nm pentacene cap layer and remain visible (indicated by black arrows in Figure 3c) but can be completely covered by thicker pentacene films (cf. Supporting Information, Figure S3).

The different resulting morphologies emphasize in particular the influence of steps on film growth. Once they are covered, the interterrace diffusion is largely reduced which in turn causes increased film roughness. Such a situation is found for the 2D and 1D C_{60} structures, while the formation of 0D clusters results in sufficient residual step edge regions which are noncovered and therefore allow efficient interterrace diffusion,

resulting in pentacene layers of higher coherence (exact numbers on the coverage and residual step edge regions of the different structures are presented in the Supporting Information).

To determine the molecular orientation within the capping layer, the application of X-ray diffraction is only of limited use because of its large probe depth, and the diffractograms are therefore mostly governed by the crystalline ordering of the supporting bottom layer. However, it allowed exclusion of the existence of crystalline pentacene islands with recumbent molecular orientation (data presented in Supporting Information, Figure S5). To reliably support our finding that the subsequently deposited pentacene molecules also adopt an upright orientation, NEXAFS measurements were carried out (cf. Figure 3d, additional spectra in Supporting Information Figure S6). Because of the low mean free path of the detected Auger electrons, this technique is inherently surface-sensitive and therefore allows determination of the average molecular orientation in the capping layer by analyzing the dichroism of the NEXAFS signatures due to excitations into the unoccupied π^* orbitals.[45] In the case of pentacene, characteristic π^* resonances appear at typical energies of 283−288 eV. As shown in Figure 3d, the intensity of these resonances is largest for perpendicular orientation of the light E-vector with respect to the sample surface normal (blue spectra) in all discussed cases, which indicates that in all cases pentacene molecules are in an upright orientation. A detailed analysis of the dichroism enabled a quantitative determination of the tilt angle (more information on the evaluation and experimental details in Supporting Information).

Except for pentacene capping layers that were deposited on the 2D C_{60} layer, average molecular tilt angles of about 85° were obtained. This value is in excellent agreement with the orientation adopted in (001)-oriented crystalline films (86°) and reflects high crystalline ordering of the capping layer. The somewhat smaller average tilt angle of 71° found for pentacene layers grown on the 2D fullerene film is in good congruence with findings of an MD study by Muccioli et al.,[34] where a significantly reduced tilt angle of pentacene after deposition onto a homogeneous C_{60} layer was reported as well as an experimental study by Dougherty et al.[46] On the other hand, one has to consider that the 2D fullerene layer does not represent a single crystalline film but contains vacancies and other defects that cause pinning of pentacene. They reduce the crystalline ordering and create notable film roughness, as was found before for pentacene films grown on polycrystalline gold substrates.[45] Therefore, the structural imperfection prevents a clear conclusion.

CONCLUSION

In summary, we have demonstrated for the case of C_{60}/pentacene heterostructures that in addition to energetic aspects, such as adhesion and cohesion energies of the individual compounds, which has been considered to rationalize the stability and possible intermixture of heterostructures,[14,15] the dynamics upon deposition are decisive for the resulting film structures. By adjustment of the substrate temperature during growth, the effective diffusion length is tuned and a site specific nucleation is achieved that allows or suppresses C_{60} nucleation at step edges or even activates diffusion along step edges yielding separated but edge-pinned C_{60} clusters. As a result, C_{60}-adlayer structures of different dimensionality have been realized ranging from planar films (2D) to step decorated chains (1D) to clusters (0D). Interestingly, all structures are found to be fully stable at room temperature. It is further demonstrated that such 1D and 0D C_{60} structures can be overgrown by subsequent pentacene deposition, forming a crystalline cover layer of the same orientation as the bottom layer, hence enabling the formation of low dimensional buried organic heterostructures. The present approach of gaining structural control over nanostructures by utilizing the anisotropic interaction between different molecular compounds and tuning the effective diffusion length is not restricted to monolayer films. It thus appears to be a rather versatile route to fabricating well ordered artificial molecular heterostructures that are necessary to explore the coupling at organic acceptor/donor interfaces and also serve as benchmark systems for detailed growth simulations.

ASSOCIATED CONTENT

Supporting Information

Additional information about the experimental setup for NEXAFS measurements and additional AFM, SEM, XRD, and NEXAFS data. This material is available free of charge via the Internet at http://pubs.acs.org.

AUTHOR INFORMATION

Corresponding Author

*E-mail: gregor.witte@physik.uni-marburg.de.

Notes

The authors declare no competing financial interest.

ACKNOWLEDGMENTS

We acknowledge support by the Deutsche Forschungsgemeinschaft (Grant SFB 1083, TP A2), the Helmholtz-Zentrum Berlin (electron storage ring BESSY II) for provision of synchrotron radiation at beamline HE-SGM, and M. Hellwig (WZMW Marburg) for his assistance with the SEM measurements. T.B. gratefully acknowledges financial support by the Friedrich-Ebert-Stiftung.

REFERENCES

(1) Yoffe, A. D. *Adv. Phys.* **2008**, *50*, 1−208.
(2) Huang, Y.; Lieber, C. M. *Pure Appl. Chem.* **2004**, *76*, 2051−2068.
(3) Schreiber, F. *Prog. Surf. Sci.* **2000**, *65*, 151−256.
(4) Love, J. C.; Estroff, L. A.; Kriebel, J. K.; Nuzzo, R. G.; Whitesides, G. M. *Chem. Rev.* **2005**, *105*, 1109−1169.
(5) Kittelson, D. B. *J. Aerosol Sci.* **1998**, *29*, 575−588.
(6) Shan, J.; Tenhu, H. *Chem. Commun.* **2007**, *44*, 4580−4598.
(7) Gaucher, G.; Dufresne, M. H.; Sant, V. P.; Kang, N.; Maysinger, D.; Leroux, J. C. *J. Controlled Release* **2005**, *109*, 169−188.
(8) Barth, J. V.; Costantini, G.; Kern, K. *Nature* **2005**, *437*, 671.
(9) Treier, M.; Fasel, R. *Chimia* **2009**, *63*, 122.
(10) Lukas, S.; Witte, G.; Wöll, Ch. *Phys. Rev. Lett.* **2002**, *88*, 028301.
(11) Xiao, W.; Ruffieux, P.; Ait-Mansour, K.; Gröning, O.; Palotas, K.; Hofer, W. A.; Gröning, P.; Fasel, R. *J. Phys. Chem. B* **2006**, *111*, 21394−21398.
(12) Wang, J.; Kaur, I.; Diaconescu, B.; Tang, J.-M.; Miller, G. P.; Pohl, K. *ACS Nano* **2011**, *5*, 1792−1797.
(13) Götzen, J.; Lukas, S.; Birkner, A.; Witte, G. *Surf. Sci.* **2011**, *605*, 577−581.
(14) Hinderhofer, A.; Schreiber, F. *ChemPhysChem* **2012**, *13*, 628.
(15) Kitaigorodsky, A. I. *Mixed Crystals*; Springer Series in Solid-State Sciences, Vol. *33*; Springer-Verlag: Berlin, 1984.
(16) Breuer, T.; Witte, G. *J. Chem. Phys.* **2013**, *138*, 114901.
(17) Heutz, S.; Cloots, R.; Jones, T. S. *Appl. Phys. Lett.* **2000**, *77*, 3938.

(18) Koller, G.; Berkebile, S.; Krenn, J. R.; Netzer, F. P.; Oezelt, M.; Haber, T.; Resel, R.; Ramsey, M. G. *Nano Lett.* **2006**, *6*, 1207−1212.
(19) Chen, W.; Qi, D. C.; Huang, H.; Gao, X.; Wee, A. T. S. *Adv. Funct. Mater.* **2011**, *21*, 410−424.
(20) Salzmann, I.; Duhm, S.; Heimel, G.; Rabe, J. P.; Koch, N.; Oehzelt, M.; Sakamoto, Y.; Suzuki, T. *Langmuir* **2008**, *24*, 7294−7298.
(21) Hinderhofer, A.; Frank, C.; Hosokai, T.; Resta, A.; Gerlach, A.; Schreiber, F. *J. Chem. Phys.* **2011**, *134*, 104702.
(22) Skabara, P.; Arlin, J.-B.; Geerts, Y. H. *Adv. Mater.* **2013**, *25*, 1948−1954.
(23) Sariciftci, N. S. *Prog. Quantum Electron.* **1995**, *19*, 131−159.
(24) Yoo, S.; Domercq, B.; Kippelen, B. *Appl. Phys. Lett.* **2004**, *85*, 5427−5429.
(25) Congreve, D. N.; Lee, J.; Thompson, N. J.; Hontz, E.; Yost, S. R.; Reusswig, P. D.; Bahlke, M. E.; Reineke, S.; Van Voorhis, T.; Baldo, M. A. *Science* **2013**, *340*, 334−337.
(26) Noever, S. J.; Fischer, S.; Nickel, B. *Adv. Mater.* **2013**, *25*, 2147−2151.
(27) Salzmann, I.; Duhm, S.; Opitz, R.; Johnson, R. L.; Rabe, J. P.; Koch, N. *J. Appl. Phys.* **2008**, *104*, 114518.
(28) Zhang, Y.; Pregler, S. K.; Myers, J. D.; Ouyang, J.; Sinnott, S. B.; Xue, J. *J. Vac. Sci. Technol.* **2009**, *B27*, 169.
(29) Jin, W.; Dougherty, D. B.; Cullen, W. G.; Robey, S.; Reutt-Robey, J. E. *Langmuir* **2009**, *25*, 9857.
(30) Smerdon, J. A.; Rankin, R. B.; Greeley, J. P.; Guisinger, N. P.; Guest, J. R. *ACS Nano* **2013**, *7*, 3086−3094.
(31) Conrad, B. R.; Tosado, J.; Dutton, G.; Dougherty, D. B.; Jin, W.; Bonnen, T.; Schuldenfrei, A.; Cullen, W. G.; Williams, E. D.; Reutt-Robey, J. E.; Robey, S. W. *Appl. Phys. Lett.* **2009**, *95*, 213302.
(32) Cantrell, R. A.; Clancy, P. *Surf. Sci.* **2008**, *602*, 3499.
(33) Cantrell, R. A.; James, C.; Clancy, P. *Langmuir* **2011**, *27*, 9944.
(34) Muccioli, L.; D'Avino, G.; Zannoni, C. *Adv. Mater.* **2011**, *23*, 4532.
(35) Fu, Y. T.; Risko, C.; Bredas, J. L. *Adv. Mater.* **2013**, *25*, 878.
(36) Yi, Y. P.; Coropceanu, V.; Bredas, J. L. *J. Am. Chem. Soc.* **2009**, *131*, 15777.
(37) Verlaak, S.; Beljonne, D.; Cheyns, D.; Rolin, C.; Linares, M.; Castet, F.; Cornil, J.; Heremans, P. *Adv. Funct. Mater.* **2009**, *19*, 3809.
(38) In analogy to the classification of geometric bodies, we consider isolated C60 clusters as 0D islands. While this terminology is consistent with the categorization of quantum dots, we note that there are also other classifications in which clusters are considered as small 3D objects.[22]
(39) Tao, C.; Stasevich, T. J.; Cullen, W. G.; Einstein, T. L.; Williams, E. D. *Nano Lett.* **2007**, *7*, 1495.
(40) Bouchoms, I. P. M.; Schoonveld, W. A.; Vrijmoeth, J.; Klapwijk, T. M. *Synth. Met.* **1999**, *104*, 175.
(41) Witte, G.; Hänel, K.; Söhnchen, S.; Wöll, Ch. *Appl. Phys. A: Mater. Sci. Process.* **2006**, *82*, 447−455.
(42) Note that the nominal thickness of the C_{60} layer that is determined by QCM reflects the thickness of an idealized film formed by layer-by-layer growth, which can differ quite substantially from the actual height of the C_{60} islands because the strong dewetting leads to a nonuniform height distribution. Nevertheless the nominal thickness is a significant value because it is directly proportional to the number of deposited molecules.
(43) Note that the diffusivity of one compound on the other does not depend on the interaction strength but rather on the lateral corrugation of the interaction potential, i.e., the difference in energy correlated to changes of the relative lateral positions of both compounds. As the geometrical corrugation is smallest for the (001) plane of pentacene and as the size mismatch between neighboring pentacene molecules (4−5 Å) and the rather large van der Waals diameter of C_{60} (about 10 Å) causes an effective averaging (due to simultaneous interaction with several pentacene molecules), this yields an overall weak corrugation and thus large diffusivity of C_{60} on uprightly oriented pentacene. For other relative orientations of pentacene and C_{60}, enhanced corrugation and therefore reduced diffusivity can be expected, which is in good congruence with our observations.
(44) Käfer, D.; Witte, G.; Wöll, Ch. *Appl. Phys. A: Mater. Sci. Process.* **2009**, *95*, 273−284.
(45) Käfer, D.; Ruppel, K.; Witte, G. *Phys. Rev. B* **2007**, *75*, 085309.
(46) Dougherty, D.; Jin, W.; Cullen, W. G.; Reutt-Robey, J. E.; Robey, S. W. *Appl. Phys. Lett.* **2009**, *94*, 023103.